

Angle Feedback for NOMA Transmission in mmWave Drone Networks

Nadisanka Rupasinghe, Yavuz Yapıcı, İsmail Güvenç, Monisha Ghosh and Yuichi Kakishima

Abstract—In this paper, we consider an unmanned aerial vehicle (UAV) based wireless network using non-orthogonal multiple access (NOMA) transmission in millimeter-wave frequencies to deliver broadband data in a spectrally efficient fashion at hotspot scenarios. The necessity for the NOMA transmitter to gather information on user channel quality becomes a major drawback in practical deployments. We therefore consider various limited feedback schemes for NOMA transmission, to relieve the complexity of tracking and feeding back the full channel state information (CSI) of the users. In particular, through beamforming we allow NOMA to exploit the space domain, and hence the user angle emerges as a promising (yet novel) limited feedback scheme. We show that as the user region for NOMA transmission gets wider, the users become more distinctive at the transmitter side with respect to their angles, making user angle feedback a better alternative than distance feedback in such scenarios. We rigorously derive and analyze the outage sum rate performance for NOMA transmission considering various user ordering strategies involving full CSI, angle, and distance feedback schemes. Our analytical results for NOMA outage sum rates using those feedback schemes match closely with simulations, and provide useful insights on properly choosing a limited feedback scheme for different deployment geometries and operating configurations.

Index Terms—5G, drone, HPPP, mmWave, non-orthogonal multiple access (NOMA), stadium, UAV.

I. INTRODUCTION

Unmanned aerial vehicles (UAVs) serving as aerial base stations (BSs) is emerging as a cost-effective and efficient solution for providing rapid on-demand connectivity during temporary events and after disasters [1]–[4]. There have been several recent use cases where UAVs were deployed as aerial BSs for providing temporary connectivity. For example, AT&T had recently deployed their flying cell on wings (COW) to provide data, voice, and text services to users in Puerto Rico in the aftermath of hurricane Maria [5], [6]. During this deployment, the UAV-BS was providing LTE connectivity to users in an area of up to 40-square mile to restore the wireless network. Nokia and British mobile operator EE have been flying small quadcopter drone BSs in Scotland since 2016, to provide instant LTE coverage using drone BSs over a disaster area with radius of about 31 miles [7]. Further, AT&T has been recently exploring the possibility of deploying UAV-BSs

for augmenting their network capacity especially in hot spot scenarios, while Ericsson considers use of drone BSs as a viable solution to provide on-demand coverage in an area with bad signal specifically for music festivals [7].

Due to the limited energy resources on board of a UAV, achieving higher spectral efficiency (SE) is of paramount importance to reap maximum benefits from UAV based communication networks. In this regard, integrating non-orthogonal multiple access (NOMA) to UAV-BSs can be an effective solution to improve their SE [8]. In contrast to the conventional orthogonal multiple access (OMA) schemes (e.g., time-division multiple access (TDMA)), NOMA simultaneously serves multiple users in the same time, frequency, code or space resources in a non-orthogonal fashion by considering power domain for multiple access. Hence, UAV-BSs can serve multiple users simultaneously with NOMA using the same resources while enhancing the achievable SE.

Use of NOMA techniques to improve SE has been studied extensively in the literature in a broader context. In particular, NOMA with multi-antenna transmission techniques has been recently receiving higher attention [4], [9]–[14]. In [9] multiple-input-multiple-output (MIMO) techniques are introduced to NOMA transmission along with user pairing and power allocation strategies to enhance MIMO-NOMA performance over MIMO-OMA. A general MIMO-NOMA framework applicable to both downlink (DL) and uplink (UL) transmission is proposed in [10] by considering signal alignment concepts. A random beamforming approach for millimeter (mmWave) NOMA networks is proposed in [11]. In that, for user ordering, full channel state information (CSI) of users which depend on the angle offset between the randomly generated base station (BS) beam, user distances and small scale fading are considered. Two users are then served simultaneously within a single beam by employing NOMA. Recently, 3rd generation partnership project group (3GPP) has also been investigating to including NOMA in the next generation communication standards [15], [16].

Use of NOMA to support UAV communications has recently been explored in the literature. A UAV based mobile cloud computing system is proposed in [17], where UAVs, using NOMA transmission, offer computation offloading opportunities to mobile stations (MS) with limited local processing capabilities. In [18], without considering any multi-antenna techniques, two user NOMA transmission is introduced to fixed-wing type UAV acting as an aerial BS. In that, the UAV-BS moves in a circular trajectory around the center of a macrocell without altering its altitude. Power allocation and UAV altitude optimization approach is proposed in [19]

N. Rupasinghe, Y. Yapıcı, and İ. Güvenç are with the Department of Electrical and Computer Engineering, North Carolina State University, Raleigh, NC, 27606 (e-mail: {rprupasi,yyapici,iguvenç}@ncsu.edu).

Monisha Ghosh is with the Department of Computer Science, University of Chicago, Chicago, IL (e-mail: monisha@uchicago.edu).

Yuichi Kakishima was with DOCOMO Innovations, Inc., Palo Alto, CA, 94304 (e-mail: yuichi.kakishima.vc@nttdocomo.com).

This research was supported in part by NSF under the grant CNS-1618692.

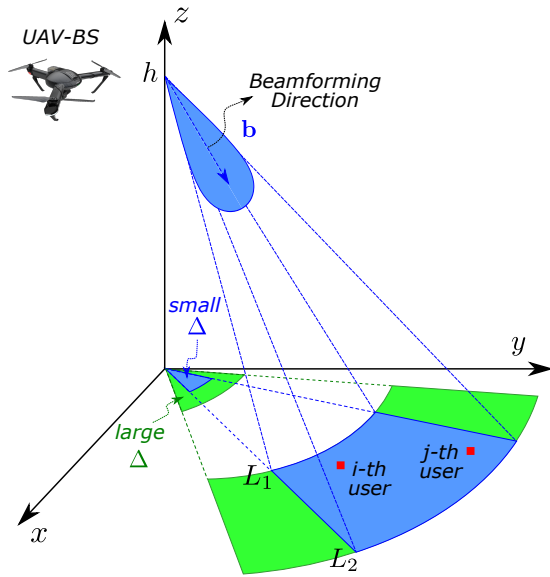


Fig. 1: System scenario of UAV-BS serving multiple users simultaneously in a single DL beam with NOMA transmission. The horizontal angle Δ is illustrated by relatively *small* and *large* angle values.

to maximize achievable NOMA sum rates in a UAV based communication network. In [20] max-min rate optimization problem is formulated for a scenario where single antenna UAV-BS is serving ground users employing NOMA transmission. In that, joint optimization of power, bandwidth, UAV altitude and antenna beamwidth is considered. In our earlier work [4], [13], NOMA is introduced to UAVs acting as aerial BSs to provide coverage over a stadium or a concert scenario. In particular, leveraging multi-antenna techniques a UAV-BS generates directional beams, and multiple users are served within the same beam employing NOMA transmission, i.e., reusing space resources. In [4] we assume the availability of full CSI feedback whereas in [13] the availability of only user distance information is assumed as a practical feedback scheme for NOMA formulation.

In this paper, which is a significantly extended version of [21], we leverage the user angle information as a measure of user channel quality for mmWave NOMA communications. In particular, employing beamforming along with mmWave transmission allows NOMA to exploit space domain and as a result user angle information becomes a promising practical alternative for full CSI feedback. To the best of the authors' knowledge, this novel strategy has not been studied in the literature before. Compared to the conventional limited feedback scheme based on users' distance (to the transmitter), the angle information is shown to have a significant potential in providing better separation for NOMA users in the power domain, and hence achieve considerably higher sum rates in many scenarios. In particular, the contributions of this work can be outlined as follows.

- We first introduce the angle based limited feedback scheme as an alternative to the full CSI and distance feedback mechanisms. We show that the optimal use of the angle information while ordering users is to employ the Fejér kernel function, which fully captures the contribution of angle in the effective channel gain. Furthermore,

absolute angle is also proposed as a more insightful yet suboptimal alternative to Fejér kernel based ordering.

- We rigorously analyze the outage probability and sum rate performance of the user ordering strategies under consideration. In particular, we propose a unified expression for the conditional outage probability, where the contribution of the ordered distance, (absolute) angle, and Fejér kernel distributions are explicitly provided. The respective ordered distributions are derived rigorously, as well, employing stochastic geometry and order statistics.
- We compare the performance of distance and angle based limited feedback and ordering strategies for various user region geometries. We show that as the users become more *distinctive* based on their angle information (i.e., wider user regions), the angle feedback scheme and respective ordering strategies (i.e., absolute angle and Fejér kernel based ordering) significantly outperforms the classical distance based feedback and ordering.

The rest of the paper is organized as follows. Section II presents the system model while limited feedback schemes and respective user ordering strategies for NOMA are discussed in Section III. In Section IV NOMA outage sum rates are analyzed and respective numerical results are presented in Section V. Finally, Section VI provides concluding remarks.

II. SYSTEM MODEL

We consider a mmWave-NOMA transmission scenario where a single UAV-BS equipped with an M element uniform linear array (ULA) is serving K single-antenna users in the DL. We assume that all these users lie inside a specific *user region*, which is identified by the inner-radius L_1 , outer-radius L_2 , and angle Δ as shown in Fig. 1. Specifically, Δ stands for the fixed angle within the projection of the horizontal beamwidth of the antenna pattern on the xy -plane. We assume that the UAV-BS generates a 3-dimensional (3D) beam \mathbf{b} as shown in Fig. 1, which is adjusted in the horizontal and vertical domains adequately to cover the user region entirely. All users are represented by the index set $\mathcal{N}_U = \{1, 2, \dots, K\}$ with the cardinality $|\mathcal{N}_U|$ being equal to K . Note that it is possible to model various different hot spot scenarios reasonably (e.g., stadium, concert hall, traffic jam, and urban canyon, etc.) by modifying these parameters.

We assume that the users are randomly distributed following a homogeneous Poisson point process (HPPP) with density λ . Hence, the number of users in the specified user region is Poisson distributed such that $P(K \text{ users in the user region}) = \frac{\mu^K e^{-\mu}}{K!}$ with $\mu = (L_2^2 - L_1^2) \frac{\Delta}{2} \lambda$.

The channel \mathbf{h}_k between the UAV-BS and user k is

$$\mathbf{h}_k = \sqrt{M} \sum_{p=1}^{N_P} \frac{\alpha_{k,p} \mathbf{a}(\theta_{k,p})}{\sqrt{\text{PL}(\sqrt{d_k^2 + h^2})}}, \quad (1)$$

where N_P , h , d_k , $\alpha_{k,p}$ and $\theta_{k,p}$ represent the number of multipaths, UAV-BS hovering altitude, horizontal distance between user k and UAV-BS, gain of the p -th path which follows standard complex Gaussian distribution with $\mathcal{CN}(0, 1)$, and

angle-of-departure (AoD) of the p -th path, respectively. The steering vector $\mathbf{a}(\theta_{k,p})$ corresponding to the AoD $\theta_{k,p}$ is defined as

$$\mathbf{a}(\theta_{k,p}) = \frac{1}{\sqrt{M}} \left[1 \ e^{-j2\pi \frac{D}{\zeta} \sin(\theta_{k,p})} \ \dots \ e^{-j2\pi \frac{D}{\zeta} \sin(\theta_{k,p})(M-1)} \right]^T,$$

where D is the antenna spacing of ULA and ζ is the wavelength. The path loss (PL) between user k and UAV-BS is captured by PL $\left(\sqrt{d_k^2 + h^2}\right)$. Without any loss of generality, we assume that all the users have line-of-sight (LoS) paths since UAV-BS is hovering at relatively high altitudes and the probability of having scatterers around UAV-BS is very small. In particular, as presented in [22], [23], the gains of Non-LoS (NLoS) paths are typically 20 dB weaker than LoS path in mmWave channels. Hence, as considered in [24], [25], it is reasonable to assume only LoS path for the mmWave channel under consideration, and (1) accordingly becomes

$$\mathbf{h}_k = \sqrt{M} \frac{\alpha_k \mathbf{a}(\theta_k)}{\sqrt{\text{PL}(\sqrt{d_k^2 + h^2})}}, \quad (2)$$

where α_k and θ_k are the complex gain and AoD of the LoS path, respectively.

III. NOMA TRANSMISSION WITH LIMITED FEEDBACK

In this section, we consider outage sum rate formulations and user ordering strategies for the NOMA transmission, which will be used within the respective derivations later in Section IV. We assume that each user has its own QoS based target rate. Further, we consider each user sends limited information back to the NOMA transmitter on its channel quality, which involves either distance or angle information of that particular user.

A. Outage Probabilities and Sum Rates

We denote the azimuth AoD value associated with the DL beam \mathbf{b} (see Fig. 1) as $\bar{\theta}$, which might be considered as *beamforming direction* for this setting, as well. Assuming that the horizontal angle Δ is small as compared to AoD values for user k (i.e., θ_k) or the DL beam (i.e., $\bar{\theta}$), we have a small angular offset such that $|\bar{\theta} - \theta_k| \rightarrow 0$. Note that in an adequate coordinate system, small angular offset always implies small individual angles such that $\sin \bar{\theta} \rightarrow \bar{\theta}$ and $\sin \theta_k \rightarrow \theta_k$. Hence, as shown in [13], using (2), the effective channel gain of user k for a particular beamforming direction $\bar{\theta}$ is given by

$$\begin{aligned} |\mathbf{h}_k^H \mathbf{b}|^2 &\approx \frac{|\alpha_k|^2}{M \times \text{PL}(\sqrt{d_k^2 + h^2})} \left| \frac{\sin\left(\frac{\pi M(\bar{\theta} - \theta_k)}{2}\right)}{\sin\left(\frac{\pi(\bar{\theta} - \theta_k)}{2}\right)} \right|^2 \\ &= \frac{|\alpha_k|^2}{\text{PL}(\sqrt{d_k^2 + h^2})} F_M(\bar{\theta} - \theta_k), \end{aligned} \quad (3)$$

where $F_M(\cdot)$ is the well-known Fejér kernel function.

We assume without any loss of generality that the users in set \mathcal{N}_U are already indexed from the best to the worst channel quality under a given criterion, where the details of ordering strategies considered in this work will be substantiated in the next section. In addition, we also assume that the NOMA

transmission targets to serve K_N users simultaneously with $K_N \leq K$, and that \mathcal{N}_N denotes the indices of NOMA users obeying the original order of \mathcal{N}_U and $\mathcal{N}_N \subset \mathcal{N}_U$.

Defining β_k as the k -th user power allocation coefficient, with $\beta_j \leq \beta_i$ for $\forall i \geq j$, $i, j \in \mathcal{N}_N$, and $\sum_{k \in \mathcal{N}_N} \beta_k^2 = 1$. The transmitted signal \mathbf{x} is generated by superposition coding as

$$\mathbf{x} = \sqrt{P_{\text{Tx}}} \mathbf{b} \sum_{k \in \mathcal{N}_N} \beta_k s_k, \quad (4)$$

where P_{Tx} and s_k with $\mathbb{E}(|s_k|^2) = 1$ are the total DL transmit power and k -th user's message, respectively. The received signal at the k -th user is then given as

$$y_k = \mathbf{h}_k^H \mathbf{x} + v_k = \sqrt{P_{\text{Tx}}} \mathbf{h}_k^H \mathbf{b} \sum_{k \in \mathcal{N}_N} \beta_k s_k + v_k, \quad (5)$$

where v_k is a zero-mean complex Gaussian noise with variance N_0 denoted as $\mathcal{CN}(0, N_0)$.

At the receiver, each user first decodes messages of all weaker users (allocated with larger power) sequentially in the presence of stronger users' messages (allocated with smaller power). Those decoded messages are then subtracted from the received signal in (5), and the user decodes its own message treating the stronger users' messages as noise. This overall decoding process is known as successive interference cancellation (SIC).

When the instantaneous rate while decoding any of the weaker users' message is larger than the QoS based target rate of that weak user, the associated decoding operation occurs without any error. Assuming that all interfering messages of users weaker than m -th user are decoded accurately (without any error), k -th user has the following signal-to-interference-plus-noise ratio (SINR) while decoding m -th user message

$$\text{SINR}_{m \rightarrow k} = \frac{P_{\text{Tx}} |\mathbf{h}_k^H \mathbf{b}|^2 \beta_m^2}{P_{\text{Tx}} \sum_{l < m, l \in \mathcal{N}_N} |\mathbf{h}_k^H \mathbf{b}|^2 \beta_l^2 + N_0}, \quad (6)$$

where $m \geq k$. Actually, (6) also represents the SINR of k -th user while decoding its own message for $m = k$. Note that the summation in the denominator of (6) disappears while k -th user being the strongest one is decoding its own message (i.e., no possible l index satisfying $l < k$ for this specific case), and we have $\frac{P_{\text{Tx}}}{N_0} |\mathbf{h}_k^H \mathbf{b}|^2 \beta_k^2$.

Defining the instantaneous rates associated with (6) to be $R_{m \rightarrow k} = \log_2(1 + \text{SINR}_{m \rightarrow k})$, the conditional outage probability of the k -th user is given as

$$\begin{aligned} P_{k|\mathcal{S}_K}^o &= 1 - \Pr \left(\bigcap_{l \geq k, l \in \mathcal{N}_N} R_{l \rightarrow k} > \bar{R}_l \mid \mathcal{S}_K \right) \\ &= 1 - \Pr \left(\bigcap_{l \geq k, l \in \mathcal{N}_N} \text{SINR}_{l \rightarrow k} > \epsilon_l \mid \mathcal{S}_K \right), \end{aligned} \quad (7)$$

where \bar{R}_k is the QoS based target rate for k -th user and $\epsilon_k = 2^{\bar{R}_k} - 1$. Note that (7) is *conditioned* over \mathcal{S}_K , which describes the given condition on K . More specifically, \mathcal{S}_K might represent either a particular integer *one at a time*, i.e., $\mathcal{S}_{K_1} = \{K \mid K = i\}$, or a range of integers *jointly*, i.e.,

$\mathcal{S}_{K_2}: \{K | j \leq K < i\}$, where $i, j \in \mathbb{Z}^+$. In other words, the outage probability in (7) corresponds to a single K value for \mathcal{S}_{K_1} , while it is associated with a range of K values jointly for \mathcal{S}_{K_2} . In Section IV, outage probability analysis will be performed specifically taking into account these two conditions of \mathcal{S}_K .

When the outage probability in (7) is obtained using \mathcal{S}_{K_1} , the outage sum rate is given as

$$R^{\text{NOMA}} = \Pr(K=1) (1 - \tilde{P}_{1|\mathcal{S}_{K_1}}^o) \bar{R}_1 + \sum_{n=2}^{\infty} \Pr(K=n) \left(\sum_{k \leq n, k \in \mathcal{N}_N} (1 - P_{k|\mathcal{S}_{K_1}}^o) \bar{R}_k \right), \quad (8)$$

where $\tilde{P}_{k|\mathcal{S}_{K_1}}^o = \Pr\left(\frac{1}{K_N} \log(1 + P_{\text{Tx}} |\mathbf{h}_k^H \mathbf{b}|^2 / N_0) < \bar{R}_k | \mathcal{S}_{K_1}\right)$ with $\tau \geq 1$ is the outage probability of k -th user during OMA transmission with the factor $\frac{1}{K_N}$ capturing the associated loss in degrees-of-freedom (DoF) gain. For comparison, we consider OMA sum rates being computed in the same way as (8), except that $P_{k|\mathcal{S}_{K_1}}^o$ in the inner summation is replaced with $\tilde{P}_{k|\mathcal{S}_{K_1}}^o$.

On the other hand, whenever (7) is obtained for a set of \mathcal{S}_{K_τ} 's with $\tau \geq 2$, where each \mathcal{S}_{K_τ} has a unique range of integers, the combined outage sum rate is described as

$$R^{\text{NOMA}} = \sum_{\tau \geq 2} \Pr\{\mathcal{S}_{K_\tau}\} \sum_{k \in \mathcal{N}_N} (1 - P_{k|\mathcal{S}_{K_\tau}}^o) \bar{R}_k = \sum_{k \in \mathcal{N}_N} (1 - P_k^o) \bar{R}_k, \quad (9)$$

where P_k^o is called the *unconditional* outage probability of k -th ($k \in \mathcal{N}_N$) user. Note that whenever we have $K_N = 1$, single user transmission is employed with full time-frequency resources and transmit power are allocated to the single user scheduled. In addition, corresponding sum rates of OMA transmission can be computed using (9) by replacing $P_{k|\mathcal{S}_{K_\tau}}^o$ with $\tilde{P}_{k|\mathcal{S}_{K_\tau}}^o$.

B. Limited Feedback Schemes and User Ordering Strategies

Since NOMA transmitter allocates power to its users based on their channel qualities, it needs to order users according to their effective channel gains given in (3). This strategy therefore requires users to send appropriate information on their respective channel qualities back to the transmitter. When the underlying channel experiences rapid fluctuations over time, tracking of the full CSI at user terminals becomes cumbersome, and frequently sending this information back to the transmitter increases link overhead. Thus, we consider two types of *limited feedback* schemes based on the 1) user distance d_k , and 2) user angle θ_k . Both distance d_k and angle θ_k information change much slowly as compared to full CSI, and are, hence, practical alternatives to full CSI feedback.

Note that the user distance d_k and angle θ_k appear in the effective channel gain expression of (3) within the individual terms $\text{PL}(\sqrt{d_k^2 + h^2})$ and $F_M(\bar{\theta} - \theta_k)$, respectively. While $\text{PL}(\cdot)$ is a monotonic function of d_k , $F_M(\cdot)$ is not monotonically varying with θ_k . Hence, distance d_k is equivalent to $\text{PL}(\sqrt{d_k^2 + h^2})$ based user ordering whereas θ_k is not equivalent to $F_M(\bar{\theta} - \theta_k)$ for ordering purpose. We therefore

consider the following optimal ordering strategies, which are based on the available limited feedback information (being the distance or angle) as follows

$$\text{Distance: } d_1 \leq d_2 \leq \dots \leq d_K, \quad (10)$$

$$\text{Fejér Kernel: } F_M(\bar{\theta} - \theta_1) \geq \dots \geq F_M(\bar{\theta} - \theta_K), \quad (11)$$

where both these ordering strategies guarantee user ordering from the best to the worst channel quality, and therefore align with the formulations in Section III-A. Although $F_M(\cdot)$ is not a monotonic function of θ_k , we will also consider the following suboptimal ordering scheme

$$\text{Angle: } \tilde{\theta}_1 \leq \tilde{\theta}_2 \leq \dots \leq \tilde{\theta}_K, \quad (12)$$

where $\tilde{\theta}_k$ is the absolute angle defined as $\tilde{\theta}_k = |\bar{\theta} - \theta_k|$. Note that, the general trend in (12) targets the ordering of users from the best to the worst channel quality. However, the channel qualities corresponding to (12) do not necessarily follow a strictly best-to-worst order since $F_M(\bar{\theta} - \theta_k)$ in (3) is not monotonic in θ_k . Nevertheless, angle based ordering strategy of (12) generally gives more insight than optimal ordering of complicated function $F_M(\bar{\theta} - \theta_k)$ as given in (11), and produces the same performance under certain circumstances which will be detailed in Section V.

C. Effect of User Ordering on Angle/Distance Distributions

In this section, we study the impact of various user ordering strategies considered in Section III-B on the distributions of user angle and distance information together with Fejér Kernel function (as a function of the angle). The conclusion of the discussion herein will be used later in Section IV while deriving exact outage sum rates for the NOMA transmission. We first consider the statistical relation between angle and distance of an arbitrary user in the following theorem.

Theorem 1: The distance and angle of an arbitrary user are statistically independent of each other given the user region and deployment scheme defined in Section II.

Proof: Consider the joint CDF of the distance d_k and angle θ_k of user k given as

$$F_{d_k \theta_k}(x, y) = \Pr\{d_k \leq x, \theta_k \leq y\} = \int_0^y \Pr\{d_k \leq x | \theta_k = z\} f_{\theta_k}(z) dz, \quad (13)$$

which follows directly from basic probability theorems in [26]. Recalling that users are uniformly deployed following HPPP, the probability within the integral of (13) does not depend on the instantaneous angle value z . Note that, we can geometrically interpret in Fig. 13(b) that any particular θ_k value does not alter either range or distribution of the distance d_k . As a result, (13) can be manipulated as

$$F_{d_k \theta_k}(x, y) = \Pr\{d_k \leq x\} \int_0^y f_{\theta_k}(z) dz = \Pr\{d_k \leq x\} \Pr\{\theta_k \leq y\}, \quad (14)$$

which shows the independence of distance d_k and angle θ_k , and hence completes the proof. ■

We now consider the impact of ordering strategies of Section III-B on the distance and angle distributions, where the

ordering is performed based on the type of limited feedback information (either distance or angle). In Fig. 2, we depict the PDF of the distance and angle of the j -th user associated with the ordering of users based on distance, Fejér Kernel, and angle given by (10), (11), and (12), respectively. We observe in Fig. 2(a) that the PDF of the ordered distance follows unordered distribution whenever the ordering strategy depends solely on angle (i.e., Fejér Kernel and angle ordering), and alters if distance ordering strategy is utilized. Similarly, the PDF of the angle in Fig. 2(b) does not change when the distance ordering strategy is employed, and alters whenever one of the angle based ordering strategies (i.e., Fejér Kernel and angle ordering) is employed. Note that, although we do not show explicitly due to space limitations, the above conclusion for the angle distribution also applies to Fejér Kernel distribution, as expected.

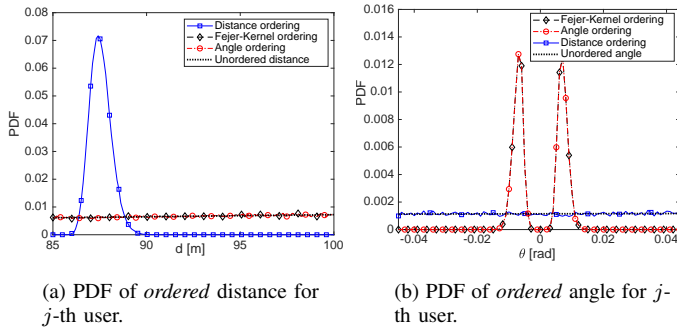


Fig. 2: PDF of *ordered* distance and angle of j -th user for the limited feedback based ordering strategies of Section III-B with $\Delta = 5^\circ$ and $j = 20$.

IV. ANALYSIS OF NOMA OUTAGE SUM RATES

In this section, we analytically investigate the outage sum rates of the NOMA transmission described in Section III-A under the limited feedback based ordering strategies of Section III-B and the full CSI based ordering. Without loss of generality, we consider two NOMA users (i.e., $K_N = 2$) in the analysis though the results can be generalized to multiple NOMA users, as well. In particular, in [15] 3GPP has studied NOMA implementation for LTE Release-13 under the name Multi-User Superposed Transmission (MUST). As defined in that, MUST-near UE (strong user) needs to be informed about paired MUST-far UE (weak user) in *physical downlink shared channel* (PDSCH) along with their transmission power allocations whereas MUST-far UE needs to know only its own power allocation.

A. Preliminaries for Outage Sum Rate Analysis

We assume that NOMA transmission targets i -th and j -th users with $i > j$, which are designated as the weaker and stronger users, respectively. In order to start transmission, there should be at least j users (i.e., $K \geq j$), while NOMA transmission requires $K \geq i$ to have both i -th and j -th users simultaneously. Whenever we have $j \leq K < i$, there is only j -th user available and all resources are allocated to this user as per single user transmission approach.

Having defined the notations \mathcal{S}_{K_1} and \mathcal{S}_{K_2} in Section III-A, we further define $\mathcal{S}_{K_3} : \{K | K \geq i\}$ here, as well, to represent the set of K values specifically enabling NOMA transmission. Note that sum rate calculation for \mathcal{S}_{K_1} is performed using (8) whereas that for \mathcal{S}_{K_2} and \mathcal{S}_{K_3} is achieved employing (9), where both formulations make use of the conditional outage probability in (7). Unless otherwise stated, $\bar{\theta}$ is set to 0 in the rest of the paper, which corresponds to the choice of a proper coordinate system as discussed in Section III-A.

Following the approach in [13], the conditional outage probability of the k -th user given in (7) can be expressed as

$$P_{k|\mathcal{S}_K}^o = \int_{u_{\min}}^{u_{\max}} \int_{L_1}^{L_2} \Pr \left\{ |\mathbf{h}_k^H \mathbf{b}|^2 < \eta_k \mid d_k = r, g(\theta_k) = u \right\} \times f_{d_k|\mathcal{S}_K}(r) f_{g(\theta_k)|\mathcal{S}_K}(u) dr du, \quad (15)$$

where $u_{\min} = \min(g(\theta_k))$, $u_{\max} = \max(g(\theta_k))$, and η_k is the variable to be specified for each NOMA user in the following. In (15), $f_{d_k|\mathcal{S}_K}(r)$ represents the distance distribution of the k -th user, and $f_{g(\theta_k)|\mathcal{S}_K}(u)$ captures distribution of either angle or Fejér Kernel (as a function of angle) of the k -th user. Note that these two PDFs are written separately in (15) as per Theorem 1, and will be derived in the subsequent sections for each NOMA user and ordering strategy separately.

When the outage probabilities are obtained individually for particular K values as represented by \mathcal{S}_{K_1} (as in the full CSI or Fejér Kernel based orderings), the outage sum rate can be computed directly using (15) in (8). On the other hand, if the outage probabilities are computed for a range of K values jointly as for \mathcal{S}_{K_2} and \mathcal{S}_{K_3} (as in the distance or angle based orderings), we need to first determine unconditional outage probabilities P_k^o using (15) for each NOMA user k , and then compute (9) accordingly.

Note that i -th user is present only for \mathcal{S}_{K_3} where $K \geq i$, and the respective unconditional outage probability is therefore given considering (9) as follows

$$P_i^o = 1 - \Pr\{\mathcal{S}_{K_3}\} \left(1 - P_{i|\mathcal{S}_{K_3}}^o\right). \quad (16)$$

Since j -th user is present for both \mathcal{S}_{K_2} and \mathcal{S}_{K_3} , the desired unconditional outage probability is obtained similarly as follows

$$P_j^o = 1 - \left[\Pr\{\mathcal{S}_{K_2}\} \left(1 - P_{j|\mathcal{S}_{K_2}}^o\right) + \Pr\{\mathcal{S}_{K_3}\} \left(1 - P_{j|\mathcal{S}_{K_3}}^o\right) \right]. \quad (17)$$

Note that the variable η_k in (15) is given for the i -th user as $\eta_i = \frac{\epsilon_i}{P_{\text{Tx}}/N_0}$, whereas that for j -th user is either $\eta_j = \frac{\epsilon_j}{P_{\text{Tx}}/N_0}$ or $\eta_j = \max \left\{ \frac{\epsilon_i/(P_{\text{Tx}}/N_0)}{\beta_i^2 - \beta_i^2 \epsilon_i}, \frac{\epsilon_j}{(P_{\text{Tx}}/N_0)\beta_j^2} \right\}$ depending on \mathcal{S}_{K_2} or \mathcal{S}_{K_3} , respectively [13]. Note also that, since $K \geq j$ is initially assumed for a valid transmission, we need to normalize the outage sum rates by $\Pr\{K \geq j\}$ to obtain final rate results.

B. Outage Probability for Fejér Kernel Based Ordering

We first consider Fejér Kernel ordering in (11) to derive $f_{d_k|\mathcal{S}_K}(r)$ and $f_{g(\theta_k)|\mathcal{S}_K}(u)$ for each NOMA user, and then compute (15). As explained in Section III-C, since Fejér Kernel is a function of angle, the ordered distance follows its

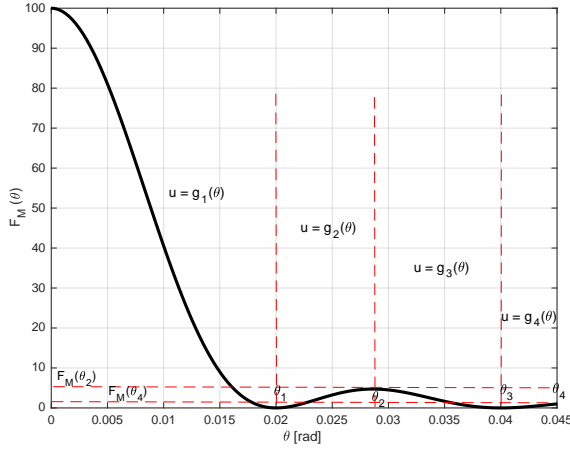


Fig. 3: Fejér Kernel function (taking values u) divided into four regions having a monotonic variation in θ with $\Delta = 5^\circ$. Respective functions over each region are $g_1(\theta)$ for $0 \leq \theta \leq \theta_1$, $g_2(\theta)$ for $\theta_1 \leq \theta \leq \theta_2$, $g_3(\theta)$ for $\theta_2 \leq \theta \leq \theta_3$ and $g_4(\theta)$ for $\theta_3 \leq \theta \leq \theta_4$.

unordered distribution while the distribution of Fejér Kernel (and equivalently that of angle) alters accordingly after ordering. Hence, we first give the distribution of the unordered distance, and then define the ordered distribution of Fejér Kernel in the following theorems.

Theorem 2: Given the user region in Section II, the PDF of the unordered user distance is

$$f_d(r) = \frac{2r}{(L_2^2 - L_1^2)}. \quad (18)$$

Proof: See Appendix A. ■

Theorem 3: The PDF of the ordered Fejér Kernel denoted for the k -th user as U_k is given by

$$f_{U_k}(z) = c_k \frac{dF_U(z)}{dz} (F_U(z))^{k-1} (1 - F_U(z))^{(K-k)}, \quad (19)$$

where U stands for the unordered Fejér Kernel and $c_k = \frac{K!}{(k-1)!(K-k)!}$. In addition, the CDF of unordered Fejér Kernel in (19) can be given specifically for $M=100$ and $\Delta = 5^\circ$ as follows

$$F_U(u) = \begin{cases} 1, & u \geq 100, \\ 1 - \frac{g_1^{-1}(u)}{\Delta/2}, & F_M(\theta_2) \leq u \leq 100, \\ \frac{g_2^{-1}(u) - g_1^{-1}(u) - g_3^{-1}(u) + \theta_4}{\Delta/2}, & F_M(\theta_4) \leq u \leq F_M(\theta_2), \\ \frac{g_2^{-1}(u) - g_1^{-1}(u) - g_3^{-1}(u) + g_4^{-1}(u)}{\Delta/2}, & u \leq F_M(\theta_4), \end{cases} \quad (20)$$

where the functions $\{g_l(u)\}_{l=1}^4$ are obtained by partitioning Fejér Kernel into smaller parts changing monotonically with respect to θ as shown in Fig. 3, and $\{\theta_l\}_{l=1}^4$ are roots of $\partial F_M(\theta)/\partial \theta$.

Proof: See Appendix B. ■

Note that the approach of Theorem 3 in deriving (20) can be generalized to any choice of M and Δ . For example, we obtain $F_U(u) = 1 - \frac{g_1^{-1}(u)}{\Delta/2}$ for $\Delta = 1^\circ$ keeping M the same. Finally, substituting $f_{d_k|S_{K_1}}(r)$ and $f_{g(\theta_k)|S_{K_1}}(u)$ with $f_d(r)$

and $f_{U_k}(z)$, respectively, and employing the distribution of $|\mathbf{h}_k^H \mathbf{b}|^2$ (exponential) [13], the outage in (15) becomes

$$P_{k|S_{K_1}}^o = \int_{u_{\min}}^{u_{\max}} \int_{L_1}^{L_2} \left(1 - e^{-\frac{\eta_k \text{PL}(\sqrt{r^2+h^2})}{u}} \right) f_{U_k}(u) f_d(r) dr du, \quad (21)$$

$$= \int_0^1 \int_{L_1}^{L_2} \left(1 - e^{-\frac{\eta_k \text{PL}(\sqrt{r^2+h^2})}{F_U^{-1}(q)}} \right) c_k q^{k-1} (1-q)^{K-k} f_d(r) dr dq, \quad (22)$$

where $k \in \{i, j\}$. Note that, (22) is obtained by substituting $q = F_U(u)$ in (19) and (21), and adjusting outer integration limit accordingly. Note also that (22) does not need the PDF of the ordered Fejér Kernel distribution, but the inverse of the unordered CDF only, which is easier to compute.

C. Outage Probability for Angle Based Ordering

We now consider angle based ordering given in (12), and derive the PDFs $f_{d_k|S_{K_1}}(r)$ and $f_{g(\theta_k)|S_{K_1}}(u)$ for each NOMA user to compute the analytical outage probability in (15). Similar to the Fejér Kernel ordering, the ordered distance follows its unordered distribution in this ordering strategy. However, the distribution of angle (and hence Fejér Kernel) alters since the ordering is performed with respect to angle, as discussed in Section III-C. Having derived the unordered distance distribution earlier in Theorem 2, we derive the PDF of the k -th user angle, θ_k , in the following theorems.

Theorem 4: Assuming that the number of users K takes values from S_{K_2} such that $j \leq K < i$, the PDF of the ordered absolute angle $\theta_k = |\theta_k|$ for the k -th user is given as

$$f_{\theta_k|S_{K_2}}(\theta) = \frac{L}{C} e^{-\frac{\Delta}{2}L} \frac{[\theta L]^{(k-1)}}{(k-1)!} \left\{ \sum_{l=0}^{i-k-1} \frac{[(\frac{\Delta}{2} - \theta)L]^l}{l!} \right\}; \theta \geq 0, \quad (23)$$

where $C = \sum_{l=j}^{i-1} \frac{e^{-\frac{\Delta}{2}L} [\frac{\Delta}{2}L]^l}{l!}$ and $L = (L_2^2 - L_1^2)\lambda$. Furthermore, if $K \in S_{K_3}$ such that $K \geq i$, we have

$$f_{\theta_k|S_{K_3}}(\theta) = \frac{L}{C} \frac{[\theta L]^{(k-1)}}{(k-1)!} \left\{ e^{-\theta L} - e^{-\frac{\Delta}{2}L} \sum_{l=0}^{i-k-1} \frac{[(\frac{\Delta}{2} - \theta)L]^l}{l!} \right\}; \theta \geq 0, \quad (24)$$

where $C = \left\{ 1 - \sum_{l=0}^{i-1} \frac{e^{-\frac{\Delta}{2}L} [\frac{\Delta}{2}L]^l}{l!} \right\}$ and $L = (L_2^2 - L_1^2)\lambda$.

Proof: See Appendix C. ■

Theorem 5: Considering the set of K values for a valid transmission such that $K \geq j$ or equivalently $K \in S_{K_2} \cup S_{K_3}$, the PDF of the ordered angle, θ_k , for the k -th user is given as

$$f_{\theta_k|S_{K_m}}(\theta) = \frac{1}{2} \bar{f}_{\theta_k|S_{K_m}}(|\theta|), \quad (25)$$

where $m = \{2, 3\}$, and $\bar{f}_{\theta_k|S_{K_m}}$ is given in (23) and (24).

Proof: See Appendix D. ■

Similar to (21), incorporating $f_d(r)$ and $f_{\theta_k|S_{K_m}}(\theta)$ from Theorem 2 and Theorem 5 into (15), the desired outage probability for NOMA users i and j is given as

$$P_{k|S_{K_m}}^o = \int_{-\frac{\Delta}{2}}^{\frac{\Delta}{2}} \int_{L_1}^{L_2} \left(1 - e^{-\frac{\eta_k \text{PL}(\sqrt{r^2+h^2})}{F_M(\theta)}} \right) f_{\theta_k|S_{K_m}}(\theta) f_d(r) dr d\theta, \quad (26)$$

where $k \in \{i, j\}$ and $m = \{2, 3\}$.

D. Outage Probability for Distance Based Ordering

We now consider distance ordering given in (10), and derive $f_{d_k|S_K}(r)$ and $f_{g(\theta_k)|S_K}(u)$ to compute (15) accordingly. When we order users based on the distance information, the distribution of angle (or equivalently Fejér Kernel) does not change while distance distribution alters accordingly, as discussed in Section III-C. The unordered angle actually follows a uniform distribution, and the PDF of the ordered distance is given in the following.

Lemma 1: Assuming that the number of users K takes values from S_{K_2} such that $j \leq K < i$, the PDF of the ordered distance d_k for the k -th user is given as

$$f_{d_k|S_{K_2}}(r) = \frac{\Delta \lambda r}{C} e^{-\frac{\Delta}{2} L \left[\frac{\Delta}{2} (r^2 - L_1^2) \lambda \right]^{(k-1)}} \frac{1}{(k-1)!} \times \left(\sum_{l=0}^{i-k-1} \frac{\left[\frac{\Delta}{2} (L_2^2 - r^2) \lambda \right]^l}{l!} \right) \quad (27)$$

where $C = \sum_{l=j}^{i-1} \frac{e^{-\frac{\Delta}{2} L \left[\frac{\Delta}{2} L \right]^l}}{l!}$ and $L = (L_2^2 - L_1^2) \lambda$.

Proof: See [13]. ■

Theorem 6: Further, when the number of users K obeys S_{K_3} such that $K \geq i$, the PDF of the ordered distance d_k for the k -th user is given as

$$f_{d_k|S_{K_3}}(r) = \frac{\Delta \lambda r}{C} \frac{\left[\frac{\Delta}{2} (r^2 - L_1^2) \lambda \right]^{(k-1)}}{(k-1)!} \times \left(e^{-\frac{\Delta}{2} (r^2 - L_1^2) \lambda} - e^{-\frac{\Delta}{2} L \sum_{l=0}^{i-k-1} \frac{\left[\frac{\Delta}{2} (L_2^2 - r^2) \lambda \right]^l}{l!}} \right) \quad (28)$$

where $C = 1 - \sum_{l=0}^{i-1} \frac{e^{-\frac{\Delta}{2} L \left[\frac{\Delta}{2} L \right]^l}}{l!}$ and $L = (L_2^2 - L_1^2) \lambda$.

Proof: See Appendix E. ■

Employing $f_{d_k|S_{K_m}}(r)$ given in (27) and (28), and $f_{g(\theta_k)|S_K}(u)$ being equal to $\frac{1}{\Delta}$ within the interval $[-\frac{\Delta}{2}, \frac{\Delta}{2}]$, the desired outage probability in (15) can be given as

$$P_{k|S_{K_m}}^o = \frac{1}{\Delta} \int_{-\frac{\Delta}{2}}^{\frac{\Delta}{2}} \int_{L_1}^{L_2} \left(1 - e^{-\frac{\eta_k \text{PL}(\sqrt{r^2+h^2})}{F_M(\theta)}} \right) f_{d_k|S_{K_m}}(r) dr d\theta, \quad (29)$$

where $k \in \{i, j\}$ and $m = \{2, 3\}$.

E. Outage Probability for Full CSI Based Ordering

In this section, we provide outage probabilities for full CSI (or, equivalently effective channel gain) based ordering to provide a comparison with the performance of limited feedback schemes considered so far. Note that the CDF of the

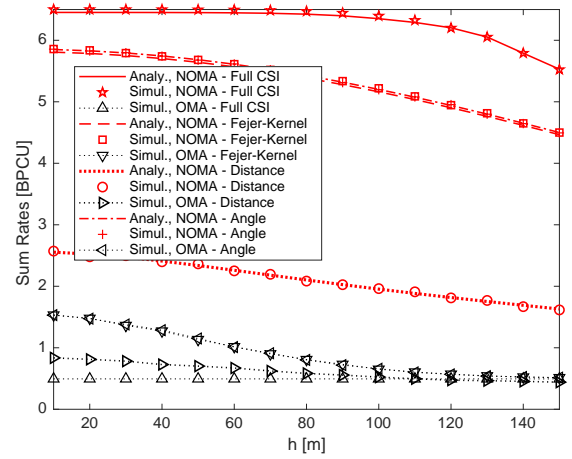


Fig. 4: Sum rates for NOMA and OMA for full CSI, Fejér kernel, distance and angle based ordering strategies with $i = 25$, $j = 20$, $P_{Tx} = 20$ dBm, and $\Delta = 5^\circ$.

unordered effective channel gain for the scenario in Section II is given as [13]

$$F_{\pi}(y) = \int_{-\frac{\Delta}{2}}^{\frac{\Delta}{2}} \int_{L_1}^{L_2} \left(1 - e^{-\frac{y \text{PL}(\sqrt{r^2+h^2})}{F_M(\theta)}} \right) \frac{r}{\frac{\Delta}{2} (L_2^2 - L_1^2)} dr d\theta, \quad (30)$$

and respective ordered CDF can be computed using order statistics, which is actually equivalent to the conditional outage probability in (15). Note that, (30) makes use of the fact that users are homogeneously distributed within the user region with the area $\mathcal{A} = \frac{\Delta}{2} (L_2^2 - L_1^2)$, and respective PDF of the user location is therefore $\frac{r}{\mathcal{A}}$ in polar coordinates.

V. NUMERICAL RESULTS

In this section, we study in detail the achievable outage sum rates with NOMA and OMA transmissions for the scenario captured in Section II. In particular, by using the derived analytical expressions in Section IV and through extensive Monte Carlo simulations we investigate the NOMA performance with various feedback schemes and user ordering strategies. Further, we study the impact of user region geometry on the NOMA feedback scheme. Unless stated otherwise, we assume that $L_1 = 85$ m, $L_2 = 100$ m, $M = 100$, $\Delta \in \{1^\circ, 5^\circ\}$, and $\bar{\theta} = 0^\circ$. Users are deployed based on HPPP with $\lambda = 1$ with respective target rates $\bar{R}_j = 6$ bits per channel use (BPCU) and $\bar{R}_i = 0.5$ BPCU. Power allocation ratios are $\beta_j^2 = 0.25$ and $\beta_i^2 = 0.75$, and the noise variance is $N_0 = -35$ dBm. The path-loss model is assumed to be $\text{PL}(\sqrt{d_k^2 + h^2}) = 1 + \left(\sqrt{d_k^2 + h^2} \right)^\gamma$ with $\gamma = 2$ [4], [11], and the UAV-BS altitude is $h \in [10, 150]$ m.

A. Performance of Ordering Strategies: NOMA vs. OMA

In Fig. 4, we present outage sum rates of OMA and NOMA along with varying UAV-BS altitudes for ordering criteria discussed in Section IV considering $i = 25$, $j = 20$, $P_{Tx} = 20$ dBm, $\Delta = 5^\circ$, and $P_{Tx} = 20$ dBm. The numerical results verify the derivations in Section IV by showing a perfect match between analytical and simulation results. In

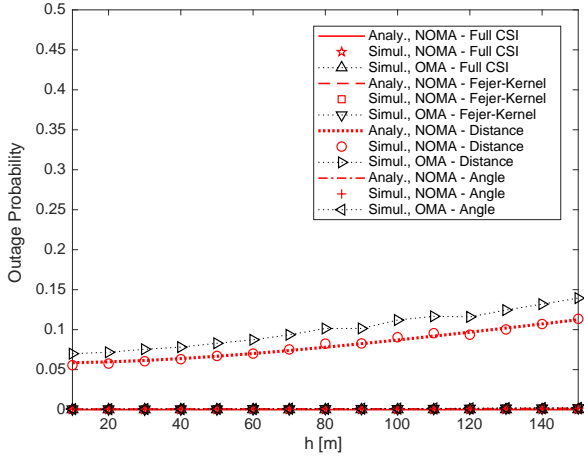
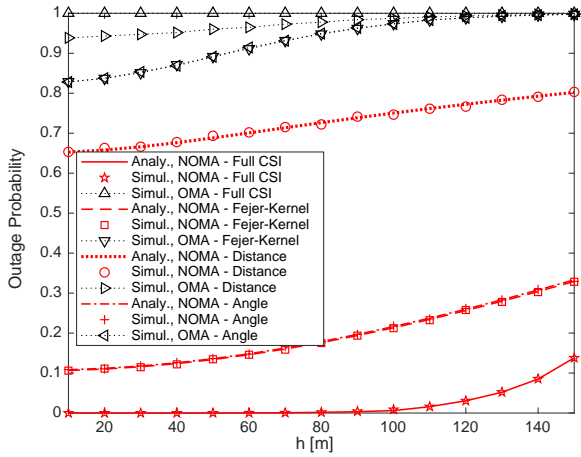
(a) i -th user with $i = 25$.(b) j -th user with $j = 20$.

Fig. 5: Outage probabilities for NOMA and OMA for full CSI, Fejér kernel, distance and angle based ordering strategies with $P_{Tx} = 20$ dBm and $\Delta = 5^\circ$.

addition, outage sum rate performance of NOMA outperforms that of OMA for all ordering criteria. We observe that sum rate performance of Fejér kernel and angle based ordering strategies are very similar (to be detailed in Section V-C), and are significantly better than that of the distance based ordering. In addition, these results are also consistent with the outage probability results presented in Fig. 5, where outage probabilities for j -th user are much more apparent.

In Fig. 6, we generate the outage sum rates for the same setting of Fig. 4, except for a narrower horizontal angle with $\Delta = 1^\circ$. We observe that Fejér kernel and angle based ordering strategies lose their power for this specific setting, and the respective sum rate performances are very similar to that of the distance based ordering. The reason for this result lies in the fact that potential NOMA users become *less distinctive* based on their angular information when Δ gets smaller. Hence, distance information might become a comparable or even more powerful feature in distinguishing different users within this setting. As a result, distance based ordering provides a relatively better power domain separation for NOMA transmission.

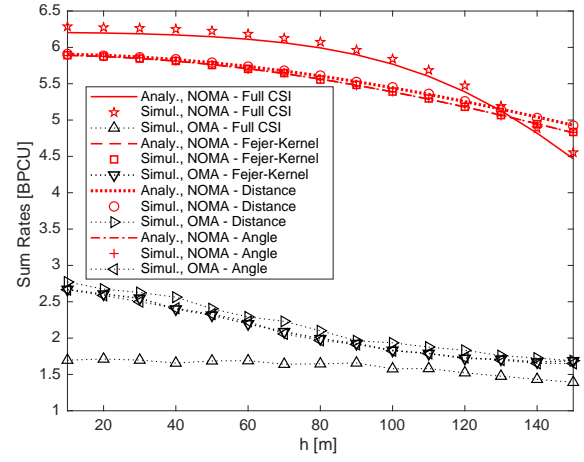


Fig. 6: Sum rates for NOMA and OMA for full CSI, Fejér kernel, distance and angle based ordering strategies with $i = 25$, $j = 20$, $P_{Tx} = 20$ dBm, and $\Delta = 1^\circ$.

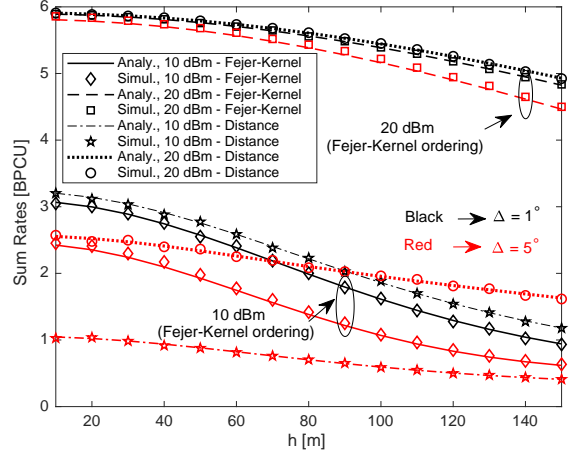


Fig. 7: NOMA sum rates for Fejér kernel and distance based ordering strategies with $i = 25$, $j = 20$, $P_{Tx} = \{10, 20\}$ dBm, and $\Delta = \{1^\circ, 5^\circ\}$.

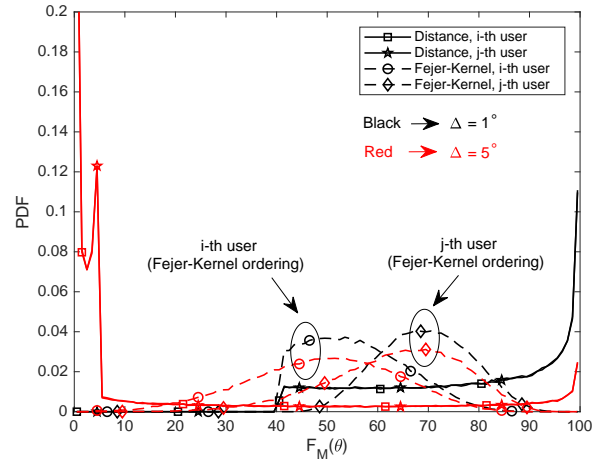


Fig. 8: PDF of Fejér kernel $F_M(\theta)$ with the distance and Fejér kernel based ordering strategies for $i = 25$, $j = 20$, and $\Delta = \{1^\circ, 5^\circ\}$.

B. Fejér Kernel vs. Distance Based Ordering

In Fig. 7 we capture NOMA outage sum rates for Fejér kernel and distance based user ordering strategies for $i = 25$, $j = 20$, $P_{Tx} = \{10, 20\}$ dBm, and $\Delta = \{1^\circ, 5^\circ\}$. From that, we

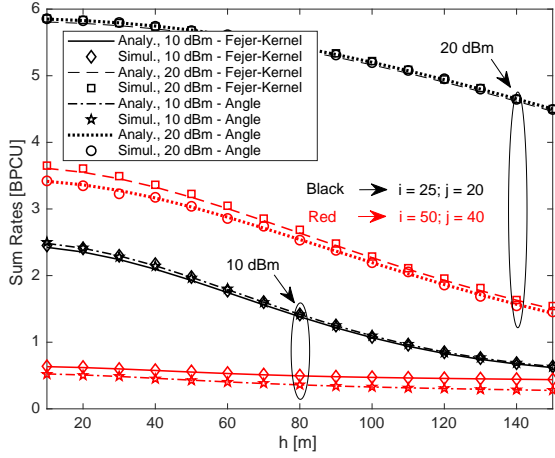


Fig. 9: NOMA sum rates for Fejér kernel and angle based ordering strategies with $\{i=25, j=20\}$, $\{i=50, j=40\}$, $P_{Tx} = \{10, 20\}$ dBm, and $\Delta = 5^\circ$.

can observe for both transmit power values fejer kernel based ordering outperforms distance based ordering for relatively larger Δ values. In particular, the sum rate performance of Fejér kernel based ordering at $P_{Tx} = 20$ dBm is significantly superior to that of the distance based ordering when $\Delta = 5^\circ$ and this difference deteriorates dramatically as Δ gets smaller.

In order to give more insights on the NOMA sum rate behavior for the Fejér kernel and distance based ordering strategies, we depict the respective PDF of Fejér kernel, $F_M(\theta)$ in Fig. 8. Note that the effective channel gain in (3) is more sensitive to variations in $F_M(\theta)$ than path-loss term, since $F_M(\theta)$ values are much bigger in magnitudes than the path-loss values. We observe that $F_M(\theta) \in [40, 100]$ for both ordering strategies when $\Delta = 1^\circ$, where the large $F_M(\theta)$ values are more probable for the distance based ordering. As a result, distance based ordering tends to achieve slightly better outage sum rate performance for $\Delta = 1^\circ$. In contrast, we have $F_M(\theta) \in [10, 90]$ for Fejér kernel based ordering when $\Delta = 5^\circ$, while respective $F_M(\theta)$ values for the distance based ordering are very likely to appear within $[0, 7]$. As a result, Fejér kernel based ordering achieves superior rate performance compared to that of distance based ordering when $\Delta = 5^\circ$.

C. Fejér Kernel vs. Angle Based Ordering

Achievable outage sum rates for NOMA considering Fejér kernel and angle based ordering are presented in Fig. 9 along with varying altitudes for $\Delta = 5^\circ$ and $P_{Tx} = \{10, 20\}$ dBm. In this case, we consider two different users pairs, 1) $i=25, j=20$, and 2) $i=50, j=40$. We observe that although both ordering strategies perform the same when $i=25$ and $j=20$, sum rate performance of the Fejér kernel based ordering becomes better as compared to angle based ordering when $i=50, j=40$. To investigate the reason behind this behavior, we plot the Fejér kernel function and the PDF of user angle θ_k in Fig. 10 considering angle based user ordering strategy.

We observe in Fig. 10 that the Fejér kernel function is decreasing monotonically (for increasing positive angles) within the support of the PDF of ordered θ_i and θ_j when $i=25$ and $j=20$. This means that the set of inequalities in the Fejér

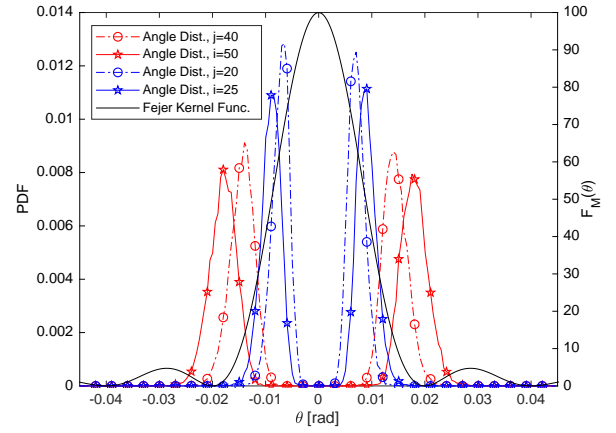


Fig. 10: PDFs of angle distribution for angle based ordering for $\Delta = 5^\circ$ with the user pairs $\{i=25, j=20\}$ and $\{i=50, j=40\}$.

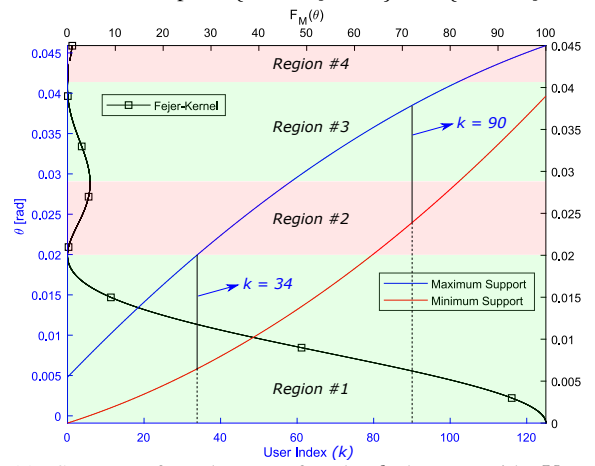


Fig. 11: Support of angle PDF for the k -th user with $K=125$, $\Delta = 5^\circ$ and angle based ordering. Entire θ support is partitioned into 4 regions in which the Fejér kernel is changing monotonically.

kernel based ordering of (11) can be equally represented by those in angle based ordering of (12). In other words, the inequality $F_M(\theta_j) \geq F_M(\theta_i)$ always corresponds to $\theta_j < \theta_i$, and, hence, both these ordering schemes become equivalent. On the other hand, when we assume the user pair $i=50$ and $j=40$, the Fejér kernel function is non-monotonic within the support of the respective angle PDFs, i.e., it increases for $\theta_k \leq 0.02$ radian and decreases for $\theta_k > 0.02$ radian (along with increasing angle). Therefore, the inequalities in Fejér kernel based ordering do not necessarily match those in absolute angle based ordering. Or equivalently, the inequality $F_M(\theta_j) \geq F_M(\theta_i)$ corresponds to either $\theta_i \geq \theta_j$ or $\theta_i < \theta_j$ depending on the particular values of θ_i and θ_j . As a result, sum rate performance of these two ordering strategy differs slightly when $i=50$ and $j=40$.

In Fig. 11, we further plot the minimum and maximum values of the support of the angle PDF, where the respective PDF is nonzero only within its support, for each user k such that $1 \leq k \leq 125$. The users are assumed to be ordered according to angle based ordering given in (12). For each angle value θ (depicted along the vertical axis), we also plot the corresponding values of the Fejér kernel function (depicted along the upper horizontal axis). In addition, we split the entire θ range into four regions, each of which guarantees monotonic variation of the Fejér kernel function (i.e., either increasing or

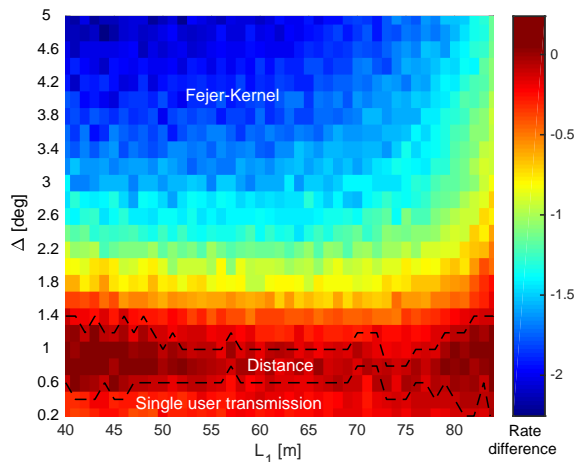
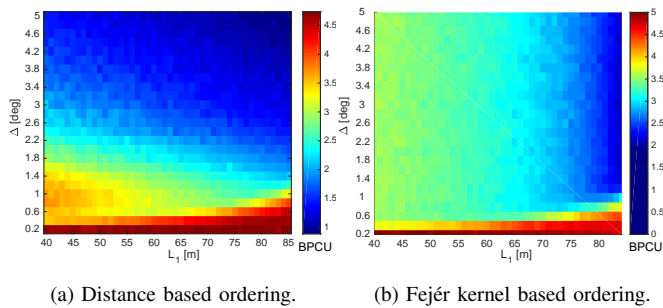


Fig. 12: Outage sum rates for various user region geometries for distance and Fejér kernel based ordering together with their difference, where $i = 25$, $j = 20$, $P_{Tx} = 10$ dBm and $h = 50$ m.

decreasing, but not both). As long as angle support of each NOMA user (i.e., both respective minimum and maximum support values) falls entirely into one of these four regions, respective $F_M(\theta)$ is guaranteed to change monotonically. In such a case, the Fejér kernel and angle based ordering strategies become equivalent. As an example, the angle support of k -th users with $k \leq 34$ completely lies within the 1st region, where $F_M(\theta)$ is a strictly decreasing function of θ . However, the angle support of user $k = 90$ lies within both the 2nd and 3rd regions, where $F_M(\theta)$ is an increasing and decreasing function of θ , respectively. Hence, as long as the NOMA user indices i and j are selected such that $j < i \leq 34$, $F_M(\theta)$ changes monotonically, and both ordering strategies achieve the same outage sum rate performance, which agrees with the results presented in Fig. 9.

D. Impact of User Region Geometry

In this section, we study the impact of different user region geometries on the outage sum rate performance of distance and Fejér kernel based ordering strategies. In particular, we consider various user regions by letting $L_1 \in [40, 85]$ m (keeping L_2 the same) and $\Delta \in [0.2^\circ, 5^\circ]$ with $i = 25$, $j = 20$, $P_{Tx} = 10$ dBm, and $h = 50$ m. The outage sum rate values are plotted in Fig. 12(a) and Fig. 12(b) for the distance and Fejér kernel ordering strategies, respectively, together with their difference in Fig. 12(c).

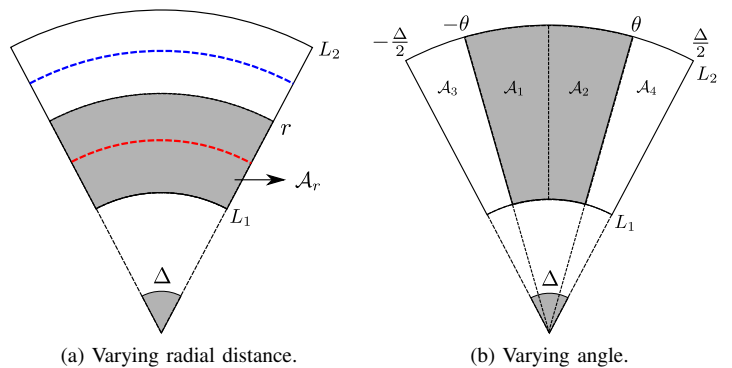


Fig. 13: Horizontal footprint of the user region in Fig. 1.

We observe that when Δ is small, distance based ordering provides greater sum rates than that of Fejér kernel, since the NOMA users can be better distinguished based on their distance (not angle) information. On the other hand, as Δ gets larger, the NOMA users become more distinctive in angle (as compared to distance) and the Fejér kernel based ordering becomes superior. This behavior actually agrees with the results of the scenario considered in Section V-B.

Note that when we have $\Delta \approx 0.2^\circ$, it is very unlikely to find both NOMA users in the user region, which basically depends on the particular choice of i and j . In this case, there is either no transmission at all, or single user transmission may happen with scheduling j -th user all the time (i.e., $j \leq K < i$). Note also that higher sum rates can be expected whenever j -th user is selected employing Fejér kernel based ordering. This is because, the contribution of $F_M(\theta)$ into the effective channel gain in (3) is higher compared to the distance dependent PL term. As a result, difference in outage sum rates in Fig. 12(c) with the label “single user transmission” appear to be negative.

VI. CONCLUDING REMARKS

In this paper, we introduce NOMA transmission along with beamforming to a UAV-BS flying over a densely packed stadium providing broadband coverage. Beamforming allows NOMA to exploit space domain and as a result user angle information becomes a promising practical alternative to full CSI feedback for NOMA formulations. Considering user angle information we propose two user ordering strategies, 1) Fejér kernel based ordering, and 2) (absolute) angle based ordering.

Our investigation shows that when determining a feedback scheme as a measure of channel quality (either angle or distance), it is important to identify under which feedback scheme users become more distinguishable. For instance, whenever the footprint of the UAV beam on the ground is wide enough in horizontal angle, the outage sum rate performance of angle based ordering strategies outperform that of the distance based user ordering. Further, we show that whenever NOMA user pair has angle support over which the Fejér kernel function is monotonically varying, both Fejér kernel and angle based ordering strategies provide similar sum rate performance.

APPENDIX A

THE PDF OF UNORDERED USER DISTANCE DISTRIBUTION

In order to derive the unordered user distance distribution, we will relate the user distances to the number of users as

discussed in [27]. In Fig. 13, we sketch the projection of 3D scenario of Fig. 1 on the horizontal plane. We observe in Fig. 13(a) that the number of users on each circular contour (having the same distance r to the origin) increases with increasing r . For example, the red contour in Fig. 13(a) is likely to have less number of users as compared to that of blue contour, since red one is shorter in length than the blue one and users are uniformly distributed. We therefore intuitively conclude that the unordered distance distribution should take larger values with increasing r , which agrees with the respective PDF in (18).

Specifically, the cumulative distribution function (CDF) of the unordered distance distribution can be written by considering average number of users in the area \mathcal{A}_r as follows

$$F_d(r) = \Pr\{d \leq r\} = \frac{\mu(\mathcal{A}_r)}{\mu} = \frac{(r^2 - L_1^2) \frac{\Delta}{2} \lambda}{(L_2^2 - L_1^2) \frac{\Delta}{2} \lambda} = \frac{(r^2 - L_1^2)}{(L_2^2 - L_1^2)}. \quad (31)$$

Taking the derivative of $F_d(r)$ we readily obtain (18). ■

APPENDIX B

THE CDF OF UNORDERED FEJÉR KERNEL

We start the derivation by splitting the Fejér Kernel function into small regions, where monotonic variation is guaranteed as shown in Fig. 3. These regions are defined as

$$\mathcal{R}_m : u = g_m(\theta) \text{ for } \{\theta_{m-1} \leq \theta \leq \theta_m\}, \quad (32)$$

where $m = 1, 2, 3, 4$, and $\theta_0 = 0$. Since Fejér Kernel function is symmetric around $\theta = 0$, it is enough to consider only one side (i.e., either $\theta < 0$ or $\theta \geq 0$) while characterizing its distribution. Recalling that U denotes unordered Fejér Kernel, the desired CDF is given as $F_U(u) = \Pr\{U \leq u\}$, which will be analyzed by considering the contribution of each region \mathcal{R}_m separately for a specific set of Fejér Kernel values.

Let us first consider the case where the Fejér Kernel value u satisfies $F_M(\theta_1) \leq u \leq 100$. We observe from Fig. 3 that the respective angle values $g_1^{-1}(u)$ (which generates specified u values) are within the region \mathcal{R}_1 only. As a result, the desired CDF for $F_M(\theta_1) \leq u \leq 100$ is given as

$$F_U(u) = \Pr\{U \leq u\} = \Pr\{\theta \geq g_1^{-1}(u)\} = 1 - \frac{g_1^{-1}(u)}{\Delta/2}. \quad (33)$$

Similarly, when u is such that $F_M(\theta_2) \leq u \leq F_M(\theta_1)$, there are three possible angle values $g_1^{-1}(u)$, $g_2^{-1}(u)$, and $g_3^{-1}(u)$ producing this specific the Fejér Kernel value u , and these angles lie within regions \mathcal{R}_1 , \mathcal{R}_2 , and \mathcal{R}_3 , respectively. The desired CDF for $F_M(\theta_2) \leq u \leq F_M(\theta_1)$ becomes

$$\begin{aligned} F_U(u) &= \Pr\{U \leq u\} \\ &= \Pr\{g_1^{-1}(u) \leq \theta \leq g_2^{-1}(u)\} + \Pr\{g_3^{-1}(u) \leq \theta \leq \theta_4\} \\ &= \frac{g_2^{-1}(u) - g_1^{-1}(u)}{\Delta/2} + \frac{\theta_4 - g_3^{-1}(u)}{\Delta/2}. \end{aligned} \quad (34)$$

Finally, whenever we have $u \leq F_M(\theta_2)$, there are four corresponding angles $g_1^{-1}(u)$, $g_2^{-1}(u)$, $g_3^{-1}(u)$, and $g_4^{-1}(u)$ lying within \mathcal{R}_1 , \mathcal{R}_2 , \mathcal{R}_3 , and \mathcal{R}_4 , respectively. The CDF for this particular condition $u \leq F_M(\theta_2)$ is given as

$$\begin{aligned} F_U(u) &= \Pr\{U \leq u\} \\ &= \Pr\{g_1^{-1}(u) \leq \theta \leq g_2^{-1}(u)\} + \Pr\{g_3^{-1}(u) \leq \theta \leq g_4^{-1}(u)\} \\ &= \frac{g_2^{-1}(u) - g_1^{-1}(u)}{\Delta/2} + \frac{g_4^{-1}(u) - g_3^{-1}(u)}{\Delta/2}, \end{aligned} \quad (35)$$

which yields (20) together with (33) and (34). ■

APPENDIX C

THE PDF OF ORDERED k -TH USER ABSOLUTE ANGLE

Since we need to have $K \geq j$ to start transmission, we derive absolute angle distribution for $\mathcal{S}_{K_2} : \{K | j < K \leq i\}$ and $\mathcal{S}_{K_3} : \{K | K \geq i\}$, separately. We first consider the CDF of the k -th user absolute angle $\tilde{\theta}_k$ for \mathcal{S}_{K_2} and $\bar{\theta} = 0$, and hence $\tilde{\theta}_k = |\theta_k|$. The CDF $F_{\tilde{\theta}_k | \mathcal{S}_{K_2}}(\theta)$ is defined as

$$F_{\tilde{\theta}_k | \mathcal{S}_{K_2}}(\theta) = \Pr\{\tilde{\theta}_k \leq \theta | j \leq K < i\} = \frac{\Pr\{\tilde{\theta}_k \leq \theta, j \leq K < i\}}{\Pr\{j \leq K < i\}}. \quad (36)$$

The denominator of (36) is readily available from the definition of HPPP, while we need to derive the probability in the numerator. For this purpose, we relate the ordered absolute angles to the number of users by making use of the geometry in Fig. 13(b). We assume that θ takes any value within the range $0 \leq \theta \leq \frac{\Delta}{2}$, and hence the entire angular range $[-\frac{\Delta}{2}, \frac{\Delta}{2}]$ is spanned by this definition. For the condition $\tilde{\theta}_k \leq \theta$ to be satisfied, it is necessary that the area $\mathcal{A}_1 \cup \mathcal{A}_2$ in Fig. 13(b) has at least k users. In addition, for a given number of users $l \geq k$ within $\mathcal{A}_1 \cup \mathcal{A}_2$, the remaining area $\mathcal{A}_3 \cup \mathcal{A}_4$ should have at most $(i - l - 1)$ users to satisfy \mathcal{S}_{K_2} (i.e., $j \leq K < i$). Equivalently, this implies that the user region should have less than i users. Hence, by considering $L = (L_2^2 - L_1^2)\lambda$, the desired probability is calculated as

$$\begin{aligned} \Pr\{\tilde{\theta}_k \leq \theta, j \leq K < i\} &= \\ &= \sum_{l=k}^{i-1} \Pr\{\mathcal{A}_1 \cup \mathcal{A}_2 \text{ has } l \text{ users, } \mathcal{A}_3 \cup \mathcal{A}_4 \text{ has at most } (i - l - 1) \text{ users}\} \\ &= \sum_{l=k}^{i-1} \frac{e^{-\theta L} [\theta L]^l}{l!} \left\{ \sum_{l'=0}^{i-l-1} \frac{e^{-(\frac{\Delta}{2} - \theta)L} [(\frac{\Delta}{2} - \theta)L]^{l'}}{l'!} \right\}. \end{aligned} \quad (37)$$

Employing $C = \Pr\{j \leq K < i\} = \sum_{l=j}^{i-1} \frac{e^{-\frac{\Delta}{2}(L_2^2 - L_1^2)\lambda} [\frac{\Delta}{2}(L_2^2 - L_1^2)\lambda]^l}{l!}$ and (37), the CDF in (36) is readily available while the respective PDF is obtained as

$$\begin{aligned} f_{\tilde{\theta}_k | \mathcal{S}_{K_2}}(\theta) &= \frac{e^{-\frac{\Delta}{2}L}}{C} \frac{d}{d\theta} \left\{ \sum_{l=k}^{i-1} \sum_{l'=0}^{i-l-1} \frac{[\theta L]^l [(\frac{\Delta}{2} - \theta)L]^{l'}}{l! l'!} \right\} \\ &= \frac{L}{C} e^{-\frac{\Delta}{2}L} \frac{[\theta L]^{(k-1)}}{(k-1)!} \left(\sum_{l=0}^{i-k-1} \frac{[(\frac{\Delta}{2} - \theta)L]^l}{l!} \right). \end{aligned} \quad (38)$$

Similarly, the CDF of k -th user absolute angle $\tilde{\theta}_k$ for \mathcal{S}_{K_3} is

$$F_{\tilde{\theta}_k | \mathcal{S}_{K_3}}(\theta) = \Pr\{\tilde{\theta}_k \leq \theta | K \geq i\} = \frac{\Pr\{\tilde{\theta}_k \leq \theta, K \geq i\}}{\Pr\{K \geq i\}}. \quad (39)$$

Considering a similar argument as in the case for \mathcal{S}_{K_2} , the probability in the numerator of (39) can be derived by relating that to the number of users in the area. In particular, $\mathcal{A}_1 \cup \mathcal{A}_2$ in Fig. 13(b) should have at least k users to satisfy $\tilde{\theta}_k \leq \theta$. Given that there are l users with $k \leq l < i$ in $\mathcal{A}_1 \cup \mathcal{A}_2$, we need to have at least $i - l$ users in the area $\mathcal{A}_3 \cup \mathcal{A}_4$ to satisfy \mathcal{S}_{K_3} (i.e., $K \geq i$). On the other hand, if $\mathcal{A}_1 \cup \mathcal{A}_2$ has more than i users, both conditions in the numerator of (39) is satisfied, and hence the desired probability can be derived as follows

$$\begin{aligned}
f_{\tilde{\theta}_k|\mathcal{S}_{K_3}}(\theta) &= \frac{d}{d\theta} F_{\tilde{\theta}_k|\mathcal{S}_{K_3}}(\theta) = \frac{1}{C} \frac{d}{d\theta} \left\{ \sum_{l=k}^{i-1} e^{-\theta L} \frac{[\theta L]^l}{l!} \right\} - \frac{e^{-\frac{\Delta}{2}L}}{C} \frac{d}{d\theta} \left\{ \sum_{l=k}^{i-1} \sum_{l'=0}^{i-l-1} \frac{[\theta L]^l \left[\left(\frac{\Delta}{2} - \theta \right) L \right]^{l'}}{l! l'} \right\} + \frac{1}{C} \frac{d}{d\theta} \left\{ 1 - \sum_{l=0}^{i-1} e^{-\theta L} \frac{[\theta L]^l}{l!} \right\} \\
&= \frac{Le^{-\theta L}}{C} \left\{ \frac{[\theta L]^{(k-1)}}{(k-1)!} - \frac{[\theta L]^{(i-1)}}{(i-1)!} \right\} - \frac{Le^{-\frac{\Delta}{2}L}}{C} \frac{[\theta L]^{(k-1)}}{(k-1)!} \left\{ \sum_{l'=0}^{i-k-1} \frac{\left[\left(\frac{\Delta}{2} - \theta \right) L \right]^{l'}}{l'} \right\} + \frac{Le^{-\theta L}}{C} \left\{ \frac{[\theta L]^{(i-1)}}{(i-1)!} \right\} \\
&= \frac{L}{C} \frac{[\theta L]^{(k-1)}}{(k-1)!} \left\{ e^{-\theta L} - e^{-\frac{\Delta}{2}L} \sum_{l=0}^{i-k-1} \frac{\left[\left(\frac{\Delta}{2} - \theta \right) L \right]^l}{l!} \right\}. \tag{41}
\end{aligned}$$

$$\begin{aligned}
\Pr\{\tilde{\theta}_k \leq \theta, K \geq i\} &= \sum_{l=k}^{i-1} \Pr\{\mathcal{A}_1 \cup \mathcal{A}_2 \text{ has } l \text{ users,} \\
&\mathcal{A}_3 \cup \mathcal{A}_4 \text{ has at least } (i-l) \text{ users}\} + \sum_{l=i}^{\infty} \Pr\{\mathcal{A}_1 \cup \mathcal{A}_2 \text{ has } l \text{ users}\}, \\
&= \sum_{l=k}^{i-1} \frac{e^{-\theta L} [\theta L]^l}{l!} \left\{ 1 - \sum_{l'=0}^{i-l-1} \frac{e^{-\left(\frac{\Delta}{2}-\theta\right)L} \left[\left(\frac{\Delta}{2} - \theta \right) L \right]^{l'}}{l'!} \right\} \\
&\quad + \left\{ 1 - \sum_{l=0}^{i-1} \frac{e^{-\theta L} [\theta L]^l}{l!} \right\}. \tag{40}
\end{aligned}$$

Employing (40) and $C = \Pr\{K \geq i\} = 1 - \sum_{l=0}^{i-1} \frac{e^{-\frac{\Delta}{2}L} \left[\frac{\Delta}{2} L \right]^l}{l!}$, the CDF in (39) is readily available. Taking the derivative of the CDF, we obtain the PDF for \mathcal{S}_{K_3} as in (41). ■

APPENDIX D

THE PDF OF ORDERED k -TH USER ANGLE DISTRIBUTION

In this section, we derive the PDF of the ordered k -th user angle distribution considering ordered the k -th user absolute angle distribution derived in Appendix C. The CDF of the ordered k -th user angle, $F_{\theta_k|\mathcal{S}_{K_m}}(\theta)$ with $m \in \{2, 3\}$ is

$$F_{\theta_k|\mathcal{S}_{K_m}}(\theta) = \Pr\{\theta_k \leq \theta | \mathcal{S}_{K_m}\}. \tag{42}$$

where $\theta \in [-\Delta, \Delta]$. In the following, we consider the desired CDF for $\theta \geq 0$ and $\theta < 0$, separately. We first consider (42) for $\theta \geq 0$. Considering Fig. 13(b), the k -th user might be in \mathcal{A}_1 , \mathcal{A}_2 , or \mathcal{A}_3 in order to satisfy $\{\theta_k \leq \theta, \theta \geq 0\}$ for a given \mathcal{S}_{K_m} . The range of values θ_k can take when the k -th user is in \mathcal{A}_1 or \mathcal{A}_2 , respectively, is given for absolute angle $\tilde{\theta}_k$ as follows

$$\begin{aligned}
\mathcal{A}_1 : & -\theta \leq \theta_k \leq 0, \\
\mathcal{A}_2 : & 0 \leq \theta_k \leq \theta, \tag{43}
\end{aligned}$$

for $0 \leq \tilde{\theta}_k \leq \theta$. Similarly, if the k -th user is in \mathcal{A}_3 or \mathcal{A}_4 , the range of θ_k values can be represented jointly as $\theta \leq \tilde{\theta}_k \leq \frac{\Delta}{2}$. With these definitions, $\Pr\{\theta_k \leq \theta, \theta \geq 0 | \mathcal{S}_{K_m}\}$ is given as

$$\begin{aligned}
\Pr\{\theta_k \leq \theta, \theta \geq 0 | \mathcal{S}_{K_m}\} &= \Pr\{\tilde{\theta}_k \leq \theta | \mathcal{S}_{K_m}\} + \frac{1}{2} \left\{ 1 - \Pr\{\tilde{\theta}_k \leq \theta | \mathcal{S}_{K_m}\} \right\} \\
&= \frac{1}{2} \left(1 + \Pr\{\tilde{\theta}_k \leq \theta | \mathcal{S}_{K_m}\} \right). \tag{44}
\end{aligned}$$

Note that, either \mathcal{A}_3 or \mathcal{A}_4 contributes equally in the probability term $\Pr\{\theta \leq \theta_k \leq \frac{\Delta}{2} | \mathcal{S}_{K_m}\}$.

We follow a similar strategy to determine $\Pr\{\theta_k \leq \theta, \theta < 0 | \mathcal{S}_{K_m}\}$ for $\theta < 0$. In particular, the k -th

user should be within \mathcal{A}_3 to satisfy $\{\theta_k \leq \theta, \theta < 0\}$ for a given \mathcal{S}_{K_m} . Then the range of values θ_k can take (when the k -th user is in \mathcal{A}_3 or \mathcal{A}_4) is given as follows

$$\begin{aligned}
\mathcal{A}_3 : & -\frac{\Delta}{2} \leq \theta_k \leq \theta, \\
\mathcal{A}_4 : & -\theta \leq \theta_k \leq \frac{\Delta}{2}, \tag{45}
\end{aligned}$$

for $-\theta \leq \tilde{\theta}_k \leq \frac{\Delta}{2}$. Hence, the desired probability is given as

$$\begin{aligned}
\Pr\{\theta_k \leq \theta, \theta < 0 | \mathcal{S}_{K_m}\} &= 0.5 \left(1 - \Pr\{\tilde{\theta}_k \leq -\theta | \mathcal{S}_{K_m}\} \right) \\
&= 0.5 \left(1 - \Pr\{\tilde{\theta}_k \leq -\theta | \mathcal{S}_{K_m}\} \right). \tag{46}
\end{aligned}$$

Using (44) and (46) in (42), CDF $F_{\theta_k|\mathcal{S}_{K_m}}(\theta)$ is given as

$$\begin{aligned}
F_{\theta_k|\mathcal{S}_{K_m}}(\theta) &= \Pr\{\theta_k \leq \theta | \mathcal{S}_{K_m}\} \\
&= \begin{cases} 0.5 \left(1 + \Pr\{\tilde{\theta}_k \leq \theta | \mathcal{S}_{K_m}\} \right), & \theta \geq 0, \\ 0.5 \left(1 - \Pr\{\tilde{\theta}_k \leq -\theta | \mathcal{S}_{K_m}\} \right), & \theta < 0, \end{cases} \\
&= 0.5 \left(1 + \text{sgn}(\theta) \Pr\{\tilde{\theta}_k \leq |\theta| | \mathcal{S}_{K_m}\} \right), \tag{47}
\end{aligned}$$

where $\text{sgn}(\cdot)$ denotes the signum function. Taking the derivative of $F_{\theta_k|\mathcal{S}_{K_m}}(\theta)$ produces the respective PDF as follows

$$\begin{aligned}
f_{\theta_k|\mathcal{S}_{K_m}}(\theta) &= \frac{d}{d\theta} F_{\theta_k|\mathcal{S}_{K_m}}(\theta) \\
&= \begin{cases} 0.5 \frac{d}{d\theta} \Pr\{\tilde{\theta}_k \leq \theta | \mathcal{S}_{K_m}\}, & \theta \geq 0, \\ -0.5 \frac{d}{d\theta} \Pr\{\tilde{\theta}_k \leq -\theta | \mathcal{S}_{K_m}\}, & \theta < 0, \end{cases} \tag{48} \\
&= \frac{\text{sgn}(\theta)}{2} \frac{d}{d\theta} \Pr\{\tilde{\theta}_k \leq |\theta| | \mathcal{S}_{K_m}\}. \tag{49}
\end{aligned}$$

Note that, $f_{\tilde{\theta}_k|\mathcal{S}_{K_m}}(\theta) = \frac{d}{d\theta} \Pr\{\tilde{\theta}_k \leq \theta | \mathcal{S}_{K_m}\}$ as derived in (38) and (41). Furthermore, following the steps in Appendix C with $\theta < 0$, we readily obtain $-f_{\tilde{\theta}_k|\mathcal{S}_{K_m}}(|\theta|) = \frac{d}{d\theta} \Pr\{\tilde{\theta}_k \leq -\theta | \mathcal{S}_{K_m}\}$. Hence, the PDF in (49) can be given for $m \in \{2, 3\}$ as follows

$$f_{\theta_k|\mathcal{S}_{K_m}}(\theta) = \frac{1}{2} f_{\tilde{\theta}_k|\mathcal{S}_{K_m}}(|\theta|). \quad \blacksquare \tag{50}$$

APPENDIX E

THE PDF OF ORDERED k -TH USER DISTANCE FOR \mathcal{S}_{K_3}

Let us first consider the cumulative distribution function (CDF) of the k -th user distance d_k assuming that K is chosen from $\mathcal{S}_{K_3} : \{K | K \geq i\}$. This can be given as

$$F_{d_k|\mathcal{S}_{K_3}}(r) = \Pr\{d_k \leq r | K \geq i\} = \frac{\Pr\{d_k < r, K \geq i\}}{\Pr\{K \geq i\}}. \tag{51}$$

Note that while the denominator of (51) is readily available from the definition of HPPP, we will relate the ordered user

$$\begin{aligned}
f_{d_k|S_{K_3}}(r) &= \frac{d}{dr} F_{d_k|S_{K_3}}(r) = \frac{1}{C} \frac{d}{dr} \left\{ \sum_{l=k}^{i-1} \frac{e^{-A_r \lambda} [\mathcal{A}_r \lambda]^l}{l!} \right\} - \frac{e^{-\frac{\Delta}{2} L}}{C} \frac{d}{dr} \left\{ \sum_{l=k}^{i-1} \sum_{l'=0}^{i-l-1} \frac{[\mathcal{A}_r \lambda]^l \left[\frac{\Delta}{2} (L_2^2 - r^2) \lambda \right]^{l'}}{l! l'} \right\} + \frac{1}{C} \frac{d}{dr} \left\{ 1 - \sum_{l=0}^{i-1} \frac{e^{-A_r \lambda} [\mathcal{A}_r \lambda]^l}{l!} \right\} \\
&= \frac{\Delta \lambda r}{C} \left\{ e^{-A_r \lambda} \left\{ \frac{[\mathcal{A}_r \lambda]^{(k-1)}}{(k-1)!} - \frac{[\mathcal{A}_r \lambda]^{(i-1)}}{(i-1)!} \right\} - \frac{e^{-\frac{\Delta}{2} L} [\mathcal{A}_r \lambda]^{(k-1)}}{(k-1)!} \left\{ \sum_{l'=0}^{i-k-1} \frac{\left[\frac{\Delta}{2} (L_2^2 - r^2) \lambda \right]^{l'}}{l'} \right\} + \frac{e^{-A_r \lambda} [\mathcal{A}_r \lambda]^{(i-1)}}{(i-1)!} \right\} \\
&= \frac{\Delta \lambda r}{C} \frac{[\mathcal{A}_r \lambda]^{(k-1)}}{(k-1)!} \left\{ e^{-A_r \lambda} - e^{-\frac{\Delta}{2} L} \sum_{l=0}^{i-k-1} \frac{\left[\frac{\Delta}{2} (L_2^2 - r^2) \lambda \right]^l}{l!} \right\}. \tag{53}
\end{aligned}$$

distances to the number of users with the help of Fig. 13(a) in order to derive the probability in the numerator. To this end, the first condition $d_k \leq r$ in the numerator of (51) is interpreted as the necessity of the area \mathcal{A}_r having at least k users. Given that there are l users with $k \leq l < i$ in \mathcal{A}_r , we need to have at least $(i-l)$ users in the rest of the area in user region to satisfy S_{K_3} (i.e., $K \geq i$). On the other hand, if \mathcal{A}_r has more than i users, both conditions in the numerator of (51) is satisfied. Letting $\mathcal{A} = \frac{\Delta}{2} (L_2^2 - L_1^2)$, the desired probability can be derived as

$$\begin{aligned}
\Pr\{d_k \leq r, K \geq i\} &= \sum_{l=k}^{i-1} \Pr\{\mathcal{A}_r \text{ has } l \text{ users,} \\
&\quad \mathcal{A} - \mathcal{A}_r \text{ has at least } (i-l) \text{ users}\} + \sum_{l=i}^{\infty} \Pr\{\mathcal{A}_r \text{ has } l \text{ users}\}, \\
&= \sum_{l=k}^{i-1} \frac{e^{-A_r \lambda} [\mathcal{A}_r \lambda]^l}{l!} \left\{ 1 - \sum_{l'=0}^{i-l-1} \frac{e^{-\frac{\Delta}{2} (L_2^2 - r^2) \lambda} \left[\frac{\Delta}{2} (L_2^2 - r^2) \lambda \right]^{l'}}{l'!} \right\} \\
&\quad + \left\{ 1 - \sum_{l=0}^{i-1} \frac{e^{-A_r \lambda} [\mathcal{A}_r \lambda]^l}{l!} \right\}. \tag{52}
\end{aligned}$$

Using (52) and $C = 1 - \sum_{l=0}^{i-1} \frac{e^{-\frac{\Delta}{2} L} \left[\frac{\Delta}{2} L \right]^l}{l!}$ with $L = (L_2^2 - L_1^2) \lambda$, the CDF in (51) can be readily obtained. Taking the derivative of (51) with respect to r , PDF can be derived as in (53). ■

REFERENCES

- [1] K. Namuduri, "When disaster strikes, flying cell towers could aid search and rescue," *IEEE Spectrum*, Aug. 2017. [Online]. Available: <https://spectrum.ieee.org/telecom/wireless/when-disaster-strikes-flying-cell-towers-could-aid-search-and-rescue>
- [2] Y. Zeng, R. Zhang, and T. J. Lim, "Wireless communications with unmanned aerial vehicles: opportunities and challenges," *IEEE Commun. Mag.*, vol. 54, no. 5, pp. 36–42, May 2016.
- [3] A. Merwaday and I. Guvenc, "UAV assisted heterogeneous networks for public safety communications," in *Proc. IEEE Wireless Communi. and Networking Conf. Workshops (WCNCW)*, March 2015.
- [4] N. Rupasinghe, Y. Yapici, I. Guvenc, and Y. Kakishima, "Non-orthogonal multiple access for mmwave drones with multi-antenna transmission," in *Proc 51st Asilomar Conf. Signal, Syst., and Comput.*, Oct 2017, pp. 958–963.
- [5] AT&T, "Flying COW connects Puerto Rico," Nov. 2017. [Online]. Available: http://about.att.com/inside_connections_blog/flying_cow_puertori
- [6] Alex Fitzpatrick, "Drones are here to stay. Get used to it," *TIME*, May. 2018. [Online]. Available: <http://time.com/longform/time-the-drone-age/>
- [7] BBC, "Drones to the rescue," May. 2018. [Online]. Available: <http://www.bbc.com/news/business-43906846>
- [8] NTT DOCOMO, Inc., "5G radio access: Requirements, concepts and technologies," Tokyo, Japan, White paper, Jul. 2014.
- [9] Z. Ding, F. Adachi, and H. V. Poor, "The application of MIMO to non-orthogonal multiple access," *IEEE Trans. Wireless Commun.*, vol. 15, no. 1, pp. 537–552, Jan. 2016.
- [10] Z. Ding, R. Schober, and H. V. Poor, "A general MIMO framework for NOMA downlink and uplink transmission based on signal alignment," *IEEE Trans. Wireless Commun.*, vol. 15, no. 6, June 2016.
- [11] Z. Ding, P. Fan, and H. V. Poor, "Random beamforming in millimeter-wave NOMA networks," *IEEE Access*, no. 99, pp. 1–1, 2017.
- [12] Z. Ding, L. Dai, and H. V. Poor, "MIMO-NOMA design for small packet transmission in the internet of things," *IEEE Access*, vol. 4, pp. 1393–1405, 2016.
- [13] N. Rupasinghe, Y. Yapici, I. Guvenc, and Y. Kakishima, "Non-orthogonal multiple access for mmwave drone networks with limited feedback," *ArXiv e-prints*, Feb. 2018. [Online]. Available: <https://arxiv.org/pdf/1801.04504.pdf>
- [14] M. Zeng, A. Yadav, O. A. Dobre, G. I. Tsiropoulos, and H. V. Poor, "Capacity comparison between MIMO-NOMA and MIMO-OMA with multiple users in a cluster," *IEEE J. Select. Areas in Commun.*, vol. 35, no. 10, Oct. 2017.
- [15] Technical Specification Group Radio Access Network, "Study on downlink multiuser superposition transmission (MUST) for LTE (Release 13)," 3GPP, Tech. Rep. 3GPP TR36.859 v13.0.0, Dec. 2015.
- [16] Y. Chen, A. Bayesteh, Y. Wu, B. Ren, S. Kang, S. Sun, Q. Xiong, C. Qian, B. Yu, Z. Ding, S. Wang, S. Han, X. Hou, H. Lin, R. Visoz, and R. Razavi, "Toward the standardization of non-orthogonal multiple access for next generation wireless networks," *IEEE Communi. Mag.*, vol. 56, no. 3, pp. 19–27, 2018.
- [17] S. Jeong, O. Simeone, and J. Kang, "Mobile edge computing via a UAV-mounted cloudlet: Optimization of bit allocation and path planning," *IEEE Trans. Vehic. Technol.*, vol. PP, no. 99, pp. 1–1, 2017.
- [18] P. K. Sharma and D. I. Kim, "UAV-enabled downlink wireless system with non-orthogonal multiple access," in *Proc. IEEE Global Commun. Conf. (GLOBECOM) workshops*, Dec 2017, pp. 1–6.
- [19] M. F. Sohail, C. Y. Leow, and S. Won, "Non-orthogonal multiple access for unmanned aerial vehicle assisted communication," *IEEE Access*, vol. 6, pp. 22 716–22 727, 2018.
- [20] A. A. Nasir, H. D. Tuan, T. Q. Duong, and H. V. Poor, "UAV-enabled communication using NOMA," *ArXiv e-prints*, June 2018. [Online]. Available: <https://arxiv.org/pdf/1806.03604.pdf>
- [21] N. Rupasinghe, Y. Yapici, I. Guvenc, and Y. Kakishima, "Comparison of limited feedback schemes for NOMA transmission in mmwave drone networks," in *Proc. IEEE Int. workshop sig. process. adv. wireless commun. (SPAWC)*, 2018 (To appear).
- [22] M. R. Akdeniz, Y. Liu, M. K. Samimi, S. Sun, S. Rangan, T. S. Rappaport, and E. Erkip, "Millimeter wave channel modeling and cellular capacity evaluation," *IEEE J. on Sel. Areas in Commun.*, vol. 32, no. 6, pp. 1164–1179, Jun. 2014.
- [23] T. S. Rappaport, E. Ben-Dor, J. N. Murdock, and Y. Qiao, "38 GHz and 60 GHz angle-dependent propagation for cellular amp; peer-to-peer wireless communications," in *Proc. IEEE Int. Conf. on Commun. (ICC)*, June. 2012, pp. 4568–4573.
- [24] G. Lee, Y. Sung, and J. Seo, "Randomly-directional beamforming in millimeter-wave multiuser MISO downlink," *IEEE Trans. Wireless Commun.*, vol. 15, no. 2, pp. 1086–1100, Feb. 2016.
- [25] D. Zhang, Z. Zhou, C. Xu, Y. Zhang, J. Rodriguez, and T. Sato, "Capacity analysis of NOMA with mmwave massive MIMO systems," *IEEE J. on Sel. Areas in Commun.*, vol. 35, pp. 1606–1618, Jul. 2017.
- [26] S. M. Ross, *Introduction to Probability Models*, 10th ed. Academic Press, 2009.
- [27] M. Haenggi, *Stochastic Geometry for Wireless Networks*. Cambridge Univ. Press, Cambridge, UK, 2012.